High-resolution quantitative whole-breast ultrasound: In vivo application using frequency-domain waveform tomography

Gursharan Yash Singh Sandhu[a], Cuiping Li[b], Olivier Roy[b], Steven Schmidt[b], Neb Duric[b,a]

[a]Department of Physics and Astronomy, Wayne State University, USA;

[b]Karmanos Cancer Institute, USA

ABSTRACT

Ultrasound tomography is a promising modality for breast imaging. Many current ultrasound tomography imaging algorithms are based on ray theory and assume a homogeneous background which is inaccurate for complex heterogeneous regions. They fail when the size of lesions approaches the wavelength of ultrasound used. Therefore, to accurately image small lesions, wave theory must be used in ultrasound imaging algorithms to properly handle the heterogeneous nature of breast tissue and the diffraction effects that it induces. Using frequency-domain ultrasound waveform tomography, we present sound speed reconstructions of both a tissue-mimicking breast phantom and *in vivo* data sets. Significant improvements in contrast and resolution are made upon the previous ray based methods. Where it might have been difficult to differentiate a high sound speed tumor from bulk breast parenchyma using ray based methods, waveform tomography improves the shape and margins of a tumor to help more accurately differentiate it from the bulk breast tissue. Waveform tomography sound speed imaging might improve the ability of finding lesions in very dense tissues, a difficult environment for mammography. By comparing the sound speed images produced by waveform tomography to MRI, we see that the complex structures in waveform tomography are consistent with those in MRI. The robustness of the method is established by reconstructing data acquired by two different ultrasound tomography prototypes.

Keywords: breast cancer, clinical breast imaging, quantitative imaging, waveform tomography

1. INTRODUCTION

Breast cancer is the second-leading cause of cancer death of American women.[1] Early detection is the best known means for reducing cancer mortality. Mammography, as a screening tool, generates many abnormal findings not related to cancer which generate additional imaging procedures. More effective screening and diagnosis tools are urgently needed for early detection of breast cancer. Tomographic imaging techniques in ultrasound show tremendous potential to detect and diagnose early stage breast cancer. In this paper, we will explore the feasibility of using frequency-domain ultrasound waveform tomography to produce high quality sound speed images of a physical breast phantom and *in vivo* data ranging from fatty to dense breasts containing tumors, parenchyma, and cysts. We will show that the improvements in contrast and resolution made upon previous ray based methods better delineate the shape and margins of structures. Thus, there is notable differentiation of benign and malignant masses from the bulk breast parenchyma. We will compare the resulting sound speed images to MRI to demonstrate concordant findings between waveform tomography and MRI. The robustness of the frequency-domain waveform tomography method is shown by producing high quality images reconstructed from data acquired by two different ultrasound tomography prototypes using ring transducer arrays.

The two ultrasound tomography prototypes considered in this work[2,3] operate in a similar fashion. A patient lies prone on the device and places their breast into ring-shaped transducer which is submerged in a water filled chamber (see Figure 1). The entire breast is then scanned from the chest wall to the nipple. The acquired data is then used to produce coronal slices of the breast. The reflected signals are used to produce tomographic B-mode

Further author information:

gursharan.sandhu@wayne.edu

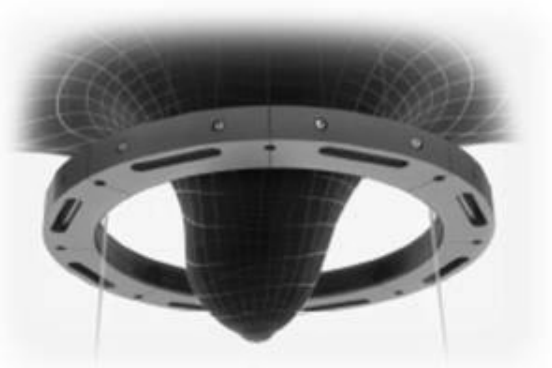

Figure 1: Placement of breast in ultrasound ring transducer array.

images while the transmitted signals are used to produce sound speed and attenuation images. The three different imaging modalities can then be used to assess breast disease. The B-mode reflection images qualitatively assess the variations in the impedance properties of the breast.[4] These images only provide morphological information which contrasts with the sound speed and attenuation images which, in addition to providing morphological information, quantitatively measure breast tissue properties. The quantitative information provided by sound speed and attenuation aids in the identification and delineation of unknown breast structures.[5,6] However, this paper will only focus on sound speed reconstruction.

Many researchers have made important advances in waveform tomography within the last decade. Geophysics researchers have demonstrated the ability of waveform tomography to image the interior of the earth with greater accuracy[7–9] (see Virieux and Operto[10] for a review). The methods contained in Pratt[9] were of critical importance for the development of our approach and algorithms. Medical applications of waveform tomography have been mostly limited to numerical data.[11–14] However, Borup *et.al.*[15] and Wiskin *et.al.*[16] have made pioneering contributions by successfully applying waveform tomography techniques to clinical *in vivo* data. Their work contrasts with ours by utilizing a planar transducer array and modeling wave propagation through an implicit integral equation technique while we use a ring transducer array and model the full wave equation, without approximation, through finite differences. We then solve the corresponding system of linear equations and update the sound speed model through gradient descent methods. Another important contribution of applying waveform tomography to *in vivo* data is given in Pratt *et.al.*[17] The authors use data acquired by our older ultrasound tomography prototype to produce sound speed and attenuation images of a tissue-mimicking breast phantom and an *in vivo* data set. They use a very similar waveform tomography algorithm, but rely on a manual travel time picker which is not a viable clinical option. In contrast, we have implemented a modified algorithm that utilizes a fully automatic approach.

2. METHOD

Two ultrasound tomography prototypes with ring array transducers were used to acquire data of a breast phantom and several *in vivo* data sets. The data was preprocessed and a subset of its frequency spectrum, up to 1 Mhz, was used as input into our frequency-domain waveform tomography algorithm. Each frequency component of the preprocessed real data is denoted $\mathbf{d}_{obs}(\omega)$ while the numerical wavefields, denoted $\mathbf{u}_{obs}(\omega, \mathbf{c})$, are created through modeling the Helmholtz equation at a particular frequency ω and current sound speed model $\mathbf{c}$ through finite differences and the solution of the corresponding system of linear equations. We then use gradient methods to iteratively solve the inverse problem to determine the unknown sound speed distribution $\mathbf{c}$ by minimizing the real valued mean squared error cost function

$$E(\omega, \mathbf{c}) = \frac{1}{2}\,\mathbf{e}^H(\omega, \mathbf{c})\,\mathbf{e}(\omega, \mathbf{c})\,,$$

where ^{H} denotes the Hermitian transpose, and $\mathbf{e}$ is the residual mismatch defined as

$$\mathbf{e}(\omega, \mathbf{c}) = \mathbf{u}_{obs}(\omega, \mathbf{c}) - \mathbf{d}_{obs}(\omega)\,.$$

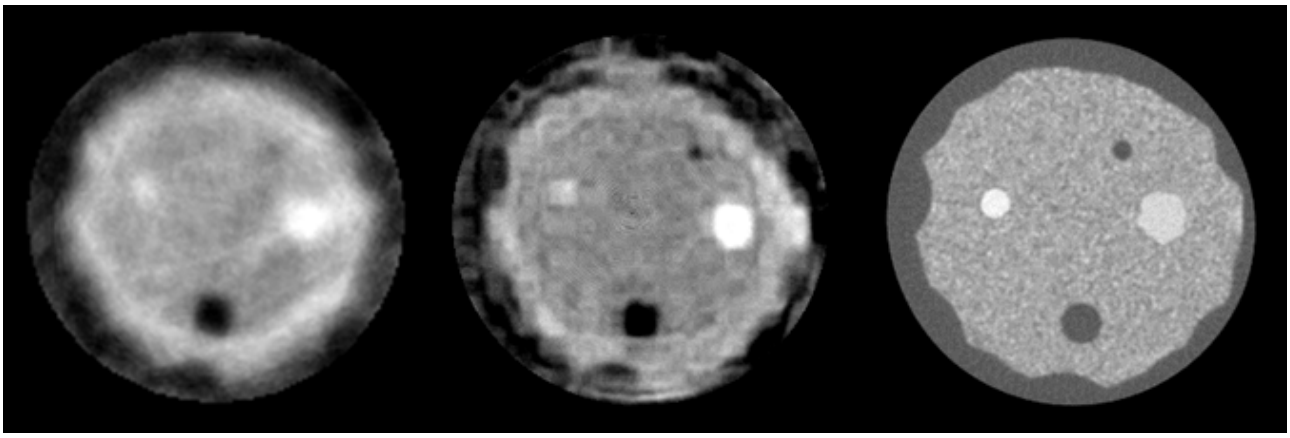

(a) (b) (c)

Figure 2: Comparison of morphology between ray based, waveform, and CT reconstruction. Data was acquired by the old prototype. (a) Ray based sound speed; (b) Waveform sound speed; (c) CT.

The update equation is given by

$$\mathbf{c}^{(i+1)} = \mathbf{c}^{(i)} - \alpha \nabla E(\omega, \mathbf{c}^{(i)}) \,,$$

where the step size α is determined by line search and the cost function gradient ∇E is taken with respect to the sound speed. In order to avoid the cycle skipping inherent in frequency-domain waveform inversion, it was essential that the ray based sound speed tomograms were used as the initial sound speed model.[5] A detailed exposition of the waveform tomography algorithm can be found in Pratt.[9] After inversion of the acoustic data, the waveform tomograms were compared to the ray based tomograms to assess the improvements that were made. The waveform tomograms were also compared to MRI to demonstrate that, for *in vivo* application, our proposed waveform tomography algorithm can achieve comparable performance.

3. RESULTS

We applied the waveform tomography algorithm to a physical breast phantom and several *in vivo* patient data sets. Comparison of the waveform tomography sound speed tomograms to the previous ray based tomograms shows that there is a measured increase in both accuracy and resolution. Comparison of the waveform tomograms to MRI shows that there is great potential for our reconstruction method to rival the performance of MRI. Numerical results as a well as a in-depth discussion of resolution analysis and computation cost can be found in our previous publication.[14]

3.1 Phantom

The ray and waveform tomography reconstructions of the sound speed distribution of a breast phantom, as well as the CT reconstruction, are shown in Figure 2. The phantom contains two high sound speed tumor inclusions and two lower sound speed fat inclusions in a background of high sound speed parenchyma. Surrounding the parenchyma is a cascading subcutaneous fat layer. The waveform tomography reconstruction shows significant improvement over the ray based reconstruction. The inclusion at 1 o'clock is not clearly visible in the ray image, but it is revealed in the waveform image. In addition, the margins of the tumors, which have critical diagnostic value,[18] are better delineated in the waveform image. A CT reconstruction corresponding to the approximate location of the sound speed images is seen in Figure 2c. The improvements made with waveform tomography sound speed imaging allows for more concordant findings with the CT reconstruction. However, this is not true in the outer edges of the waveform sound speed image in Figure 2b where there is a presence of cycle skipping artifacts. Note that the phantom was scanned by the old prototype and the images were manually masked to highlight comparison of the lesions within the phantom.

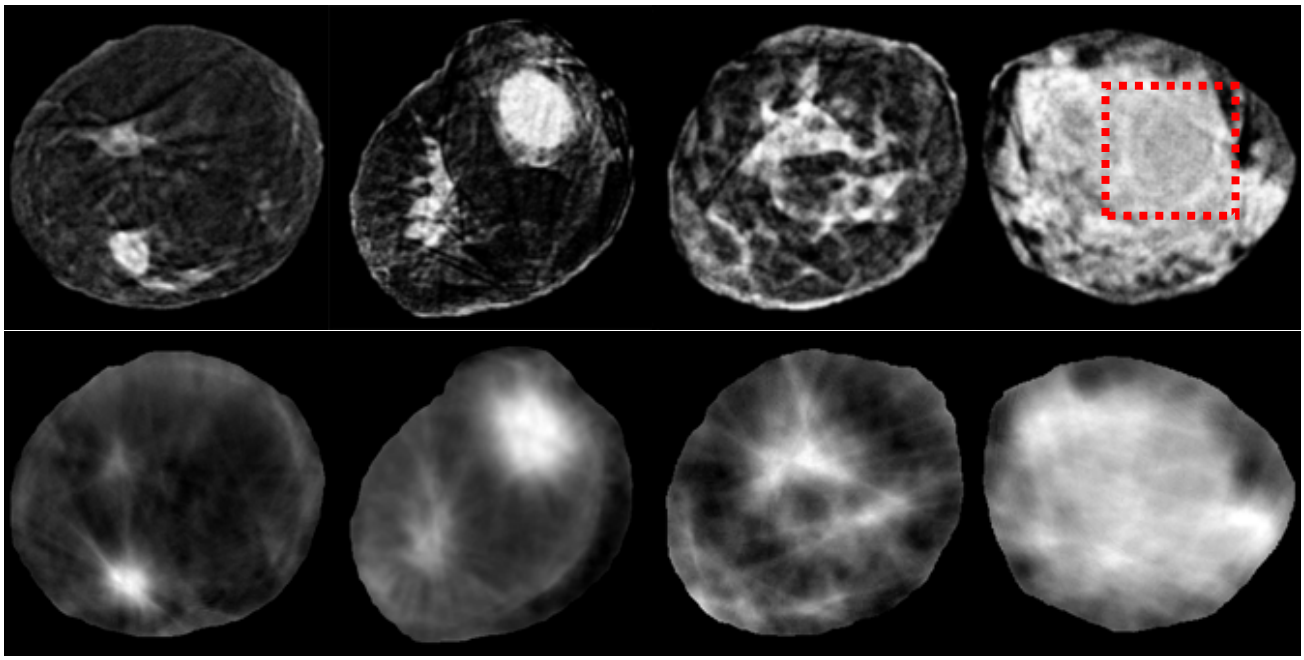

(a) (b) (c) (d)

Figure 3: Comparison of waveform tomography reconstructions to ray based reconstructions for sound speed. Data was acquired by the old prototype. (Top) Waveform Tomography. (Bottom) Ray Based. (a) Fatty breast with a IDC at 7 o'clock; (b) Scattered breast with a IDC at 1 o'clock; (c) Heterogeneous breast; (d) Extremely dense breast with a cyst at 2 o'clock. A box has been placed around the cyst to highlight its location.

3.2 In Vivo

In order to assess the clinically relevant improvements of waveform tomography over the current ray based reconstructions, we applied waveform tomography to previously acquired *in vivo* data from our old clinical prototype. The *in vivo* data spans the different breast densities found within patients. The waveform tomograms (top row), along with the corresponding ray tomograms (bottom row) are shown in Figure 3. From left to right, the breasts range from fatty to dense, spanning the 4 BI-RADS criteria for breast density. It can be seen that the outer edges of the glandular tissue (white) are sharper and have well defined edges in the waveform images. The fatty tissues (dark) and skin layers are also clearly revealed in the waveform image, whereas the tissues are poorly resolved and there is no indication of the skin in the ray based tomograms. Also, the shape and margins of the tumors, which have additional diagnostic value, are improved in the waveform tomograms. Waveform tomography also removes some of the artifacts present in ray tomography. By using waveform tomography, some of the noise induced by the ray based algorithm has been suppressed. Ray artifacts are reduced in the waveform image (though some remain because of the sparse coverage provided by the older prototype and through inheritance from the initial ray based sound speed image). Based on the patient reports, the invasive ductal carcinoma at 7 o'clock in Figure 3a has a size of 2.4 cm. Compared to the ray based reconstruction, delineation of the tumor shape and margins and overall image contrast in the waveform tomogram in Figure 3a is significantly improved. The improvements made in contrast and resolution provided by our waveform tomography algorithm will allow a radiologist to assess the physiological significance of a mass based on the shape and margins as well as its sound speed. In Figure 3b, the invasive ductal carcinoma at 1 o'clock has a size of 5.5 cm as described in the patient reports. Similar improvements can be seen in the waveform image over the ray based image. In Figure 3c, the complex shape and margins of parenchyma is clearly presented in the waveform tomogram. Figure 3d shows a large cyst at 2 o'clock embedded in extremely dense breast tissue. A box has been placed around the cyst to highlight its location. The ability to image the wall around the cyst is greatly improved over the ray based reconstruction where only a faint shadow of the cyst is present. The capability of waveform tomography to image this cyst in an extremely dense breast is very encouraging as mammography does not perform well in

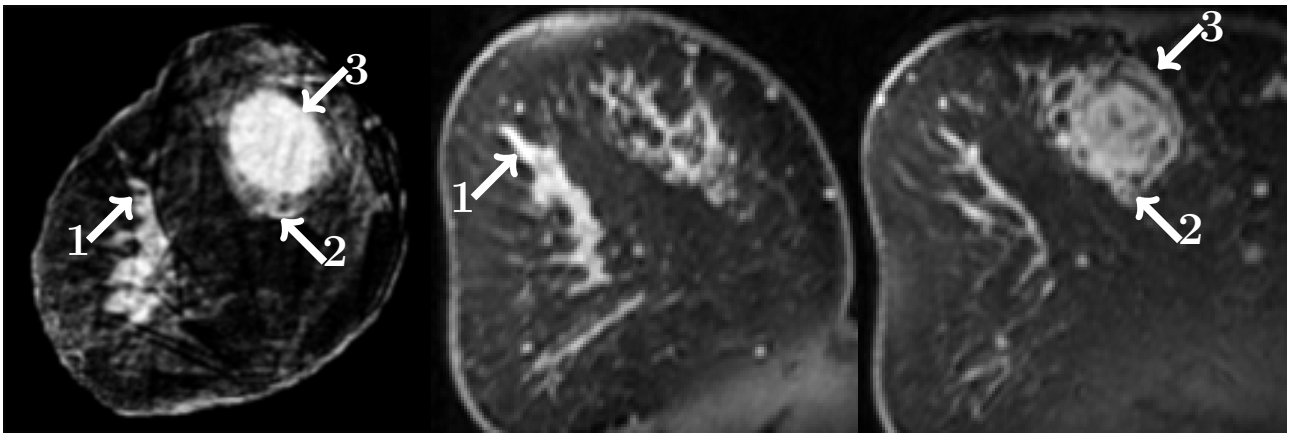

(a) (b) (c)

Figure 4: Comparison of waveform tomography reconstruction to MRI. Combinations of numbers and arrows indicate the corresponding tissues for comparison. Data was acquired by the old prototype. (a) Waveform sound speed; (b) MR slice with corresponding parenchyma; (c) MR slice with corresponding tumor.

this environment. Note that these patients were scanned by the old prototype and the images were manually masked to highlight the comparison of breast tissue.

3.3 Comparison to MRI

We compared our waveform tomograms with MRI (Figures 4 and 5 for data obtained by the old prototype; Figures 6 and 7 for data obtained by the new prototype). For the images in Figures 4, 5, 6, and 7, arrows mark some of the corresponding areas. Note that it is difficult to perfectly register the images created by both modalities. Aside from typical registration problems, it is particularly difficult in this case because the coronal slices of the waveform tomography images are at an angle with respect to MRI due to the differences in the positioning of the breast in the acquisition process. In particular, the breast is suspended in water during acquisition by our tomographic ultrasound prototype. Thus, in order to identify structures that are present in one slice of the waveform tomography image, several slices of the MRI reconstruction may be needed. Likewise, several waveform tomography images might be needed to register a single MR image. Also, waveform tomography sound speed images corresponding to the new prototype had their the gray scale values inverted to improve visualization and comparison with the particular MRI sequence that was used. Thus, for these images, darker areas correspond to regions of higher sound speed. MRI breast images were also resampled from their original transverse orientation and projected into the coronal plane to match the orientation of waveform tomography.

In Figure 4a, a large tumor is present at 1 o'clock. The shape and margins of the tumor are well reconstructed by waveform tomography. Some of the filamentary structure of the tumor is discernible. For example, the small strand at the inferior portion of the tumor is present in both Figures 4a and 4c. In addition, the shape of the dense tissue structures at 8 o'clock in Figure 4a matches well with that of MRI in Figure 4b. In Figure 5, the waveform inversion (Figure 5a) of breast parenchyma is compared to MRI (Figures 5b and 5c). The overall shape of the parenchyma matches very well. In Figures 6a and 6b, the waveform inversion reveals a small tumor at 10 o'clock. Both the tumor and filamentary structures match very well with MRI in Figure 6c. In Figure 7, very fine parenchymal structures are imaged in a very similar fashion by both waveform tomography and MRI. Overall, there is a great deal of concordance between our preliminary waveform tomography sound speed images and the well established modality of MRI. Morphological comparison of the shape of complex parenchyma and other breast features verifies the capabilities of waveform tomography to image real structures. The high quality images obtained by reconstructing both data sets highlights the robustness of the algorithm. Note that some of these patients were scanned by the older prototype while others were scanned by the new prototype. Images were manually masked to highlight the comparison of breast tissue.

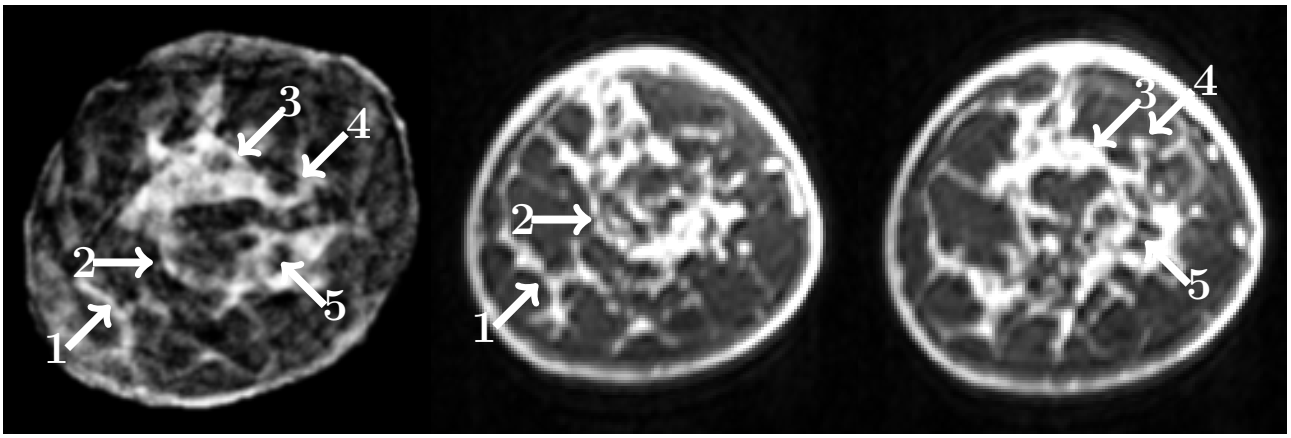

(a) (b) (c)

Figure 5: Comparison of waveform tomography reconstruction to MRI. Combinations of numbers and arrows indicate the corresponding tissues for comparison. Data was acquired by the old prototype. (a) Waveform sound speed; (b) and (c) Corresponding MRI slices.

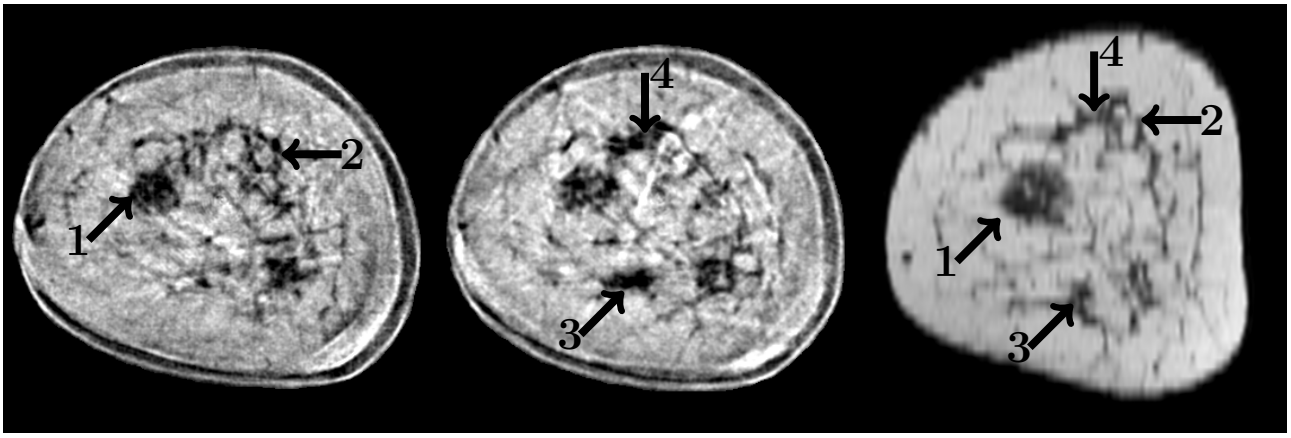

(a) (b) (c)

Figure 6: Comparison of waveform tomography reconstruction to MRI. Combinations of numbers and arrows indicate the corresponding tissues for comparison. Data was acquired by the new prototype. Gray scale values of the waveform tomography image have been inverted to better match the MR image. (a) Waveform sound speed; (b) Waveform sound speed; (c) MR slice with corresponding tumor and parencyhma.

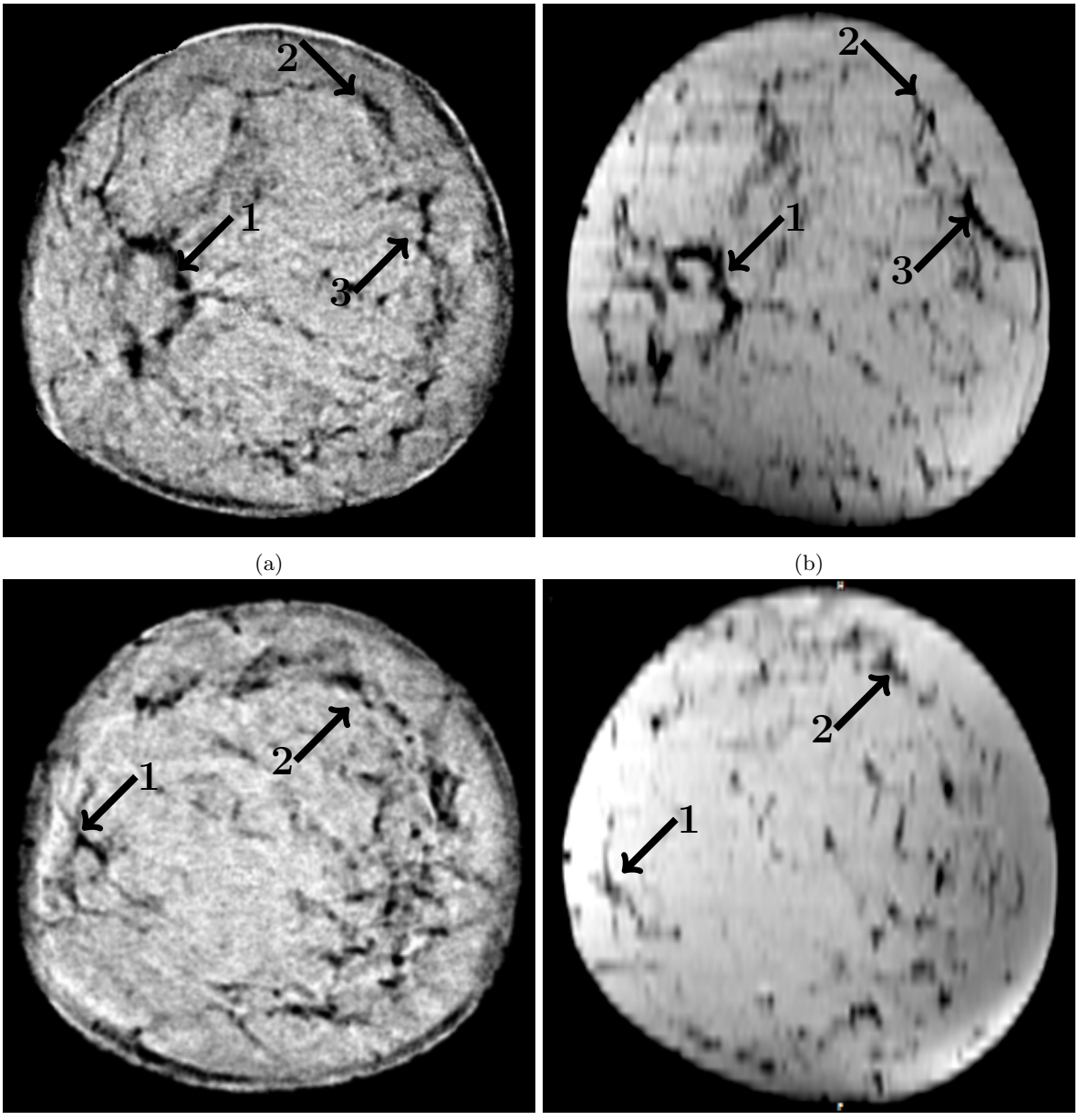

(a) (b)

(c) (d)

Figure 7: Comparison of waveform tomography reconstruction to MRI. Combinations of numbers and arrows indicate the corresponding tissues for comparison. Data was acquired by the new prototype. Gray scale values of the waveform tomography image have been inverted to better match the MR image. (a) Waveform sound speed; (b) Corresponding MRI slice; (c) Waveform sound speed; (d) Corresponding MRI slice.

4. CONCLUSIONS

We have developed a frequency-domain waveform tomography algorithm which successfully inverts acoustic data acquired by ultrasound tomography prototypes with ring transducers. The resulting high-resolution images map the sound speed distribution of breast tissue. The improvements made upon our previous ray based sound speed images are significant. The margins and shapes of tumors and other breast structures are improved which may allow a clinical observer to make a better diagnosis of the underlying breast disease. We also compared our resultant waveform tomography sound speed images to MRI to find that both modalities image breast structures in a consistent manner. In particular, the very complex shapes of breast parencyhma are very similar. The robustness of the algorithm has been established by the successful inversion of acoustic data acquired by two different ultrasound tomography prototypes with ring transducer arrays. Future work will focus on the optimization of the algorithm, reduction of the computation time, and improvements in the accuracy of the reconstruction process.

5. ACKNOWLEDGMENT

This work was partially funded by the National Institutes of Health (NIH) through National Cancer Institute grants R43CA171601 and R44CA165320.

REFERENCES

[1] DeSantis, C., Siegel, R., Bandi, P., and Jemal, A., "Breast cancer statistics, 2011," *CA: A cancer journal for clinicians* **61**(6), 408–418 (2011).

[2] Duric, N., Littrup, P., Poulo, L., Babkin, A., Pevzner, R., Holsapple, E., Rama, O., and Glide, C., "Detection of breast cancer with ultrasound tomography: First results with the computed ultrasound risk evaluation (CURE) prototype," *Medical physics* **34**(2), 773–785 (2007).

[3] Roy, O., Schmidt, S., Li, C., Allada, V., West, E., Kunz, D., and Duric, N., "Breast imaging using ultrasound tomography: From clinical requirements to system design," in [*International Ultrasonics Symposium*], 1174–1177, IEEE (2013).

[4] Schmidt, S., Duric, N., Li, C., Roy, O., and Huang, Z.-F., "Modification of Kirchhoff migration with variable sound speed and attenuation for acoustic imaging of media and application to tomographic imaging of the breast," *Medical physics* **38**(2), 998–1007 (2011).

[5] Li, C., Duric, N., and Huang, L., "Clinical breast imaging using sound-speed reconstructions of ultrasound tomography data," in [*Medical Imaging*], 692009–692009, International Society for Optics and Photonics (2008).

[6] Li, C., Duric, N., and Huang, L., "Comparison of ultrasound attenuation tomography methods for breast imaging," in [*Medical Imaging*], 692015–692015, International Society for Optics and Photonics (2008).

[7] Tarantola, A., "Inversion of seismic reflection data in the acoustic approximation," *Geophysics* **49**(8), 1259–1266 (1984).

[8] Song, Z.-M., Williamson, P. R., and Pratt, R. G., "Frequency-domain acoustic-wave modeling and inversion of crosshole data: Part II-inversion method, synthetic experiments and real-data results," *Geophysics* **60**(3), 796–809 (1995).

[9] Pratt, R. G., "Seismic waveform inversion in the frequency domain, part 1: Theory and verification in a physical scale model," *Geophysics* **64**(3), 888–901 (1999).

[10] Virieux, J. and Operto, S., "An overview of full-waveform inversion in exploration geophysics," *Geophysics* **74**(6), WCC1–WCC26 (2009).

[11] Natterer, F., "Acoustic mammography in the time domain," *University of Münster, Germany, Tech. Rep* (2008).

[12] Roy, O., Jovanović, I., Hormati, A., Parhizkar, R., and Vetterli, M., "Sound speed estimation using wave-based ultrasound tomography: theory and GPU implementation," in [*SPIE Medical Imaging*], 76290J–76290J, International Society for Optics and Photonics (2010).

[13] Huang, L., Lin, Y., Zhang, Z., Labyed, Y., Tan, S., Nguyen, N., Hanson, K., Sandoval, D., and Williamson, M., "Breast ultrasound waveform tomography: using both transmission and reflection data, and numerical virtual point sources," in [*SPIE Medical Imaging*], 90400T–90400T, International Society for Optics and Photonics (2014).

[14] Li, C., Sandhu, G. S., Roy, O., Duric, N., Allada, V., and Schmidt, S., "Toward a practical ultrasound waveform tomography algorithm for improving breast imaging," in [*SPIE Medical Imaging*], 90401P–90401P, International Society for Optics and Photonics (2014).

[15] Borup, D. T., Johnson, S. A., Natterer, F., Olsen, S. C., Wiskin, J. W., Wubeling, F., and Zhang, Y., "Apparatus and method for imaging with wavefields using inverse scattering techniques," (Dec. 21 1999). US Patent 6,005,916.

[16] Wiskin, J., Borup, D., Johnson, S., Berggren, M., Abbott, T., and Hanover, R., "Full-wave, non-linear, inverse scattering," in [*Acoustical Imaging*], 183–193, Springer (2007).

[17] Pratt, R. G., Huang, L., Duric, N., and Littrup, P., "Sound-speed and attenuation imaging of breast tissue using waveform tomography of transmission ultrasound data," in [*Medical Imaging*], 65104S–65104S, International Society for Optics and Photonics (2007).

[18] Stavros, A. T., Thickman, D., Rapp, C. L., Dennis, M. A., Parker, S. H., and Sisney, G. A., "Solid breast nodules: use of sonography to distinguish between benign and malignant lesions.," *Radiology* **196**(1), 123–134 (1995).